Received: 2 April 2020 | Revised: 2 July 2020 | Accepted: 15 July 2020

DOI: 10.1002/qj.3876

Quarterly Journal of the Royal Meteorological Society RMetS

RESEARCH ARTICLE

Overestimated acceleration of the advective Brewer–Dobson circulation due to stratospheric cooling

Roland Eichinger[1,2] | Petr Šácha[3,4]

[1]Meteorological Institute, Ludwig Maximilians University (LMU), Munich, Germany

[2]Institut für Physik der Atmosphäre, Deutsches Zentrum für Luft- und Raumfahrt (DLR), Oberpfaffenhofen, Germany

[3]Institute of Meteorology and Climatology, University of Natural Resources and Life Sciences (BOKU), Vienna, Austria

[4]Department of Atmospheric Physics, Charles University Prague, Czech Republic

Correspondence
R. Eichinger, DLR, Institut für Physik der Atmosphäre, Münchner Strasse 20, Oberpfaffenhofen, D-82234 Wessling, Germany.
Email: roland.eichinger@dlr.de

Funding information
Bayerisch-Tschechische Hochschulagentur (BTHA/BAYHOST), Grant/Award Number: BTHA-MOB-2020-2; Grantová Agentura České Republiky, Grant/Award Numbers: 16-01562J, 18-01625S; Helmholtz Association, Grant/Award Number: VH-NG-1014; MSCA-IF III, Grant/Award Number: CZ.02.2.69/0.0/0.0/19_074/0016231; Xunta de Galicia, Grant/Award Number: ED481B 2018/103

Abstract

Tropospheric warming and stratospheric cooling influence the vertical structure of the atmosphere. Numerous studies have analysed the thermal expansion of the troposphere, however, stratospheric cooling reverses the sign of this shift in the middle stratosphere, causing a downward shift in the upper stratosphere and mesosphere. This is a robust feature in transient climate model simulations, but its impact is commonly unappreciated. Here, we quantify the trend difference of the residual mean vertical velocity ($\overline{w}^*$), a proxy for diagnosing the advective Brewer–Dobson circulation (BDC) strength, which arises from implicit neglect of the shrinking distance between stratospheric pressure levels in the CCMI-1 (Chemistry-Climate Model Initiative part 1) data request. There, a log-pressure formula with constant scale height is recommended to compute $\overline{w}^*$. However, stratospheric cooling in transient climate simulations causes a reduction of the geometrical distance between pressure levels and thereby also the scale height significantly decreases over time. Using the general scale height definition for the transformation, the $\overline{w}^*$ trends are therefore smaller. In both cases, the units are $\mathrm{m{\cdot}s^{-1}}$, but in the latter case it is the constant measure of length geopotential metres and not log-pressure metres. We quantify that, due to the temperature dependence of log-pressure metres, past studies that based $\overline{w}^*$ trend analyses on log-pressure $\overline{w}^*$ overestimated the advective BDC acceleration by ~20%. This result is consistent among the CCMI-1 projections over the 1960–2100 period. We highlight that other diagnostics can also be affected by the neglect of the declining stratospheric pressure level distance. A detailed description of the diagnostics is necessary for consistent assessments of trends. Data processing tools should generally not include the constant scale height assumption if the data are used for trend analyses.

KEYWORDS

Stratosphere, Brewer-Dobson circulation, global climate modelling, vertical velocity, CCMI, scale height, climate change, coordinate system

1 | INTRODUCTION

There is robust observational evidence that the troposphere is warming and the stratosphere is cooling in response to the radiative forcing of anthropogenic greenhouse gas (GHG) emissions (IPCC, 2013). Changes in temperature directly influence the vertical structure of the atmosphere. This can be quantified via the hypsometric equation (assuming dry air and hydrostatic balance):

$$\phi(p_2) - \phi(p_1) = g_0 \cdot \{Z(p_2) - Z(p_1)\} = R \int_{p_2}^{p_1} T \, \mathrm{d}(\ln p). \tag{1}$$

Here, $\phi(p)$ is the geopotential and $Z(p)$ the geopotential height of pressure levels, $g_0 = 9.80665\,\mathrm{m{\cdot}s^{-2}}$ is the global average of gravity at mean sea level, T the temperature, p the pressure and R the gas constant for dry air ($R = 287\,\mathrm{J{\cdot}kg^{-1}{\cdot}K^{-1}}$). Equation (1) shows that the troposphere should be thermally expanding as a consequence of the positive temperature trends. This expansion has been observed and documented by means of measurements of the tropopause upward shift (Seidel and Randel, 2006). Sausen and Santer (2003) have proposed that changes in tropopause height may be a sensitive indicator of anthropogenic climate change. Gettelman *et al.* (2010), Kim *et al.* (2013) and Vallis *et al.* (2015) have shown that the tropopause rise is a robust fingerprint of climate change in simulations with comprehensive climate models. Analysing reanalysis data, Manney and Hegglin (2018) found out that it is induced through both radiative and dynamical processes.

On the one hand, the tropopause rise reflects the thermal expansion of the troposphere via Equation (1). On the other hand, the tropopause pressure is also decreasing over time, which means that the tropopause rise exceeds the vertical shift of pressure levels. Still, the increasing tropopause height is considered as a marker of the upward shift of the general circulation in the troposphere (Singh and O'Gorman, 2012) as well as in the lower stratosphere (Shepherd and McLandress, 2011). In the latter region, it partly overlaps with the robustly projected Brewer–Dobson circulation (BDC) acceleration (e.g., Oberländer-Hayn *et al.*, 2016; Abalos *et al.*, 2017; Eichinger *et al.*, 2019).

Stratospheric cooling is consistently simulated in current chemistry-climate models (CCMs; e.g., Fu *et al.*, 2004; Austin *et al.*, 2009) with regard to satellite-based and radiosonde temperature observations (e.g., Randel *et al.*, 2009; Funatsu *et al.*, 2016; Khaykin *et al.*, 2017; Maycock *et al.*, 2018). This negative temperature trend reduces the upward shift of pressure levels in the stratosphere with increasing altitude so that it even reverses sign in the middle stratosphere (Šácha *et al.*, 2019), leading to a downward shift of the upper stratosphere and mesosphere. The upward shift in the lower stratosphere together with the downward shift in the upper stratosphere result in a contraction of the stratosphere, or in other words, a reduction of stratospheric thickness. The process is even enhanced by the tropopause and stratopause shift relative to pressure levels (Laštovička *et al.*, 2006; Lübken *et al.*, 2009; Berger and Lübken, 2011; Šácha *et al.*, 2019). In the mesosphere and in the lower parts of the thermosphere, the continuing GHG-induced downward shift of the geopotential height of pressure levels influences meteor heights, satellite trajectories, orbital lifetimes, propagation of radio waves and hence the performance of space-based navigational systems (Laštovička *et al.*, 2006; Jacobi, 2014; Stober *et al.*, 2014; Lima *et al.*, 2015).

In the present paper, we report and quantify the uncertainty of advective BDC trends that arise from the implicit neglect of the stratospheric pressure level contraction using log-pressure coordinates, as is requested by the Chemistry-Climate Model Initiative part 1 (CCMI-1; Eyring *et al.*, 2013; Hegglin *et al.*, 2015; Morgenstern *et al.*, 2017). The tropical mean of the residual mean vertical velocity ($\overline{w}^*$) at a given pressure level is often taken as a proxy for diagnosing the stratospheric circulation strength (e.g., Butchart *et al.*, 2010; Abalos *et al.*, 2015; Dietmüller *et al.*, 2018). Due to the type of vertical coordinate of most climate models (σ levels), $\overline{w}^*$ is commonly converted from $\mathrm{Pa{\cdot}s^{-1}}$ to $\mathrm{m{\cdot}s^{-1}}$ units, which are traditionally used for further analyses and are then consistent among the models. The log-pressure formula (Andrews *et al.*, 1987) requested by CCMI-1 (Hegglin *et al.*, 2016) includes a constant scale height for this conversion. However, the distance between pressure levels (and the scale height) significantly decreases over time in transient climate simulations as the stratosphere cools. The temperature dependence of the scale height is made explicit when calculating the conversion using the equation of state. A key difference between the two conversion formulae is that they are related to different vertical coordinate systems – log-pressure and geopotential coordinates. It has long been known that the relationship between geometric height (or geopotential height) and log-pressure height is nonlinear (e.g., Andrews *et al.*, 1987, table 1). However, the fact that for the log-pressure height the relationship changes as the structure of the atmosphere changes (Schmidt *et al.*, 2006) has often been overlooked in the past. Using the CCMI-1 projection simulations, the present study demonstrates that, particularly for trend studies, the log-pressure formula requested in the CCMI-1 data request can be misleading.

In Section 2 of the paper, we briefly describe the analysed CCMI-1 REF-C2 model simulations. In Section 3, we explain in detail how stratospheric cooling distorts the $\overline{w}^*$ trends if the unit conversion is made with constant scale

height. In Section 4, an analysis of the CCMI-1 REF-C2 simulations is made to quantify this artificial enhancement of $\overline{w}^*$, which can be misinterpreted as BDC acceleration and, if not computed consistently, can also have an effect on the streamfunction and the tropical upward mass flux. As stratospheric cooling is a robust and strong pattern in climate projection simulations, also the trends of other diagnostics which are computed by means of a constant scale height will be influenced, and this is also the case in other multi-model projects. We discuss these points and some consequences for climate model analyses in Section 5 and end with concluding remarks in Section 6.

2 | MODEL DATA

In the present study, we analyse data from eleven CCMI-1 REF-C2 climate–chemistry simulations (only r1i1p1 ensemble members) (Eyring *et al.*, 2013; Hegglin *et al.*, 2016; Morgenstern *et al.*, 2017). The models used are:

ACCESS (Australian Community Climate and Earth System Simulator; Morgenstern *et al.*, 2009; 2013; Stone *et al.*, 2016);

CMAM (Canadian Middle Atmosphere Model; Jonsson *et al.*, 2004; Scinocca *et al.*, 2008);

CCSR/NIES (Centre for Climate System Research/ National Institute of Environmental Studies; Imai *et al.*, 2013; Akiyoshi *et al.*, 2016);

EMAC-L47, EMAC-L90 (ECHAM/MESSy Atmospheric Chemistry; Jöckel *et al.*, 2010, 2016);

GEOSCCM (Goddard Earth Observing System Chemistry Climate Model; Molod *et al.*, 2012; 2015; Oman *et al.*, 2011; 2013);

MRI (Meteorological Research Institute; Deushi and Shibata, 2011; Yukimoto *et al.*, 2011; 2012);

NIWA–UKCA (National Institute of Water and Atmospheric Research–United Kingdom Chemistry and Aerosol; Morgenstern *et al.*, 2009; 2013);

SOCOLv3 (Solar–Climate Ozone Links; Stenke *et al.*, 2013; Revell *et al.*, 2015);

ULAQ (University of L'Aquila; Pitari *et al.*, 2014); and

WACCM (Whole Atmosphere Community Climate Model; Marsh *et al.*, 2013; Solomon *et al.*, 2015).

This selection is based on the availability of the variables in the British Atmospheric Data Centre (BADC) repository we require for the analysis. In particular, we used the variables $\overline{w}^*$, temperature and geopotential height. The REF-C2 simulations cover the period 1960–2100 and follow the WMO (2011) A1 scenario for ozone-depleting substances (ODSs) and the Representative Concentration Pathway (RCP 6.0) scenario (Meinshausen *et al.*, 2011) for other greenhouse gases, tropospheric ozone (O_3) precursors, as well as aerosol and aerosol precursor emissions. For anthropogenic emissions, the recommendation was to use MACCity (Granier *et al.*, 2011) until 2000, followed by RCP 6.0 emissions. For more details on the particular models and on the model set-up, refer to Morgenstern *et al.* (2017) and citations therein.

Due to the reversal in signs of ODS and ozone trends, the year 2000 marks a change in stratospheric dynamics (Morgenstern *et al.*, 2018; Polvani *et al.*, 2018; Eichinger *et al.*, 2019). However, figures 3 and 4 in Šácha *et al.* (2019) show that, with respect to the pressure level rise, there is no substantial trend difference between shorter periods between 1960 and 2100. The multi-model mean geopotential heights at 1 hPa, at 100 hPa and their difference show no trend reversals or changes related to the periods of ODS or ozone rise and decline (see Supplementary Information). Therefore, we consider the entire period 1960–2100 for our analysis.

3 | PHYSICAL MECHANISM

As mentioned above, tropospheric warming together with stratospheric cooling lead to an upward shift of pressure levels in the troposphere (e.g., Vallis *et al.*, 2015). This upward shift reduces with altitude in the lower stratosphere and reverses sign in the middle stratosphere, resulting in a downward shift of pressure levels in the upper stratosphere and mesosphere in transient climate model simulations (Šácha *et al.*, 2019). Figure 1 shows the geopotential height trends of the EMAC-L47 CCMI-1 REF-C2 simulation from 1960 to 2100 (Jöckel *et al.*, 2016; Morgenstern *et al.*, 2017) to illustrate the shrinking distances between pressure levels in the stratosphere due to stratospheric cooling.

A positive geopotential height trend is visible in the troposphere and lower stratosphere with a maximum in the tropical tropopause region. Above the middle stratosphere, the trends are negative and the magnitude of the trend increases with altitude. This means that the pressure levels in the stratosphere move closer together. Table 1 shows the mean distance between 100 and 1 hPa and its absolute and relative trends in percentage as a proxy for the shrinking distance between stratospheric pressure levels for the REF-C2 simulations.

The multi-model-mean (MMM) climatological distance between the 1 and 100 hPa levels is 31.0 (±0.2) km in the tropical stratosphere. The distance shrinks by about 70 m per decade, which accounts for about 0.23% per decade. This is consistently simulated in the eleven REF-C2 simulations, and the inter-model standard deviations are comparably small (4 m·decade^{-1} and 0.01%·decade^{-1}).

TABLE 1 Overview of tropical (within the turnaround latitudes) distance between the 100 and the 1 hPa levels and its reduction of the CCMI-1 REF-C2 model simulations over the period 1960–2100 including the multi-model-mean (MMM) and the inter-model standard deviation (σ)

Model	Distance between 1 and 100 hPa (m)	Trend of distance (m·decade^{-1})	Trend of distance (%·decade^{-1})
WACCM	30,915	−62	−0.20
ULAQ	31,112	−76	−0.25
SOCOLv3	30,873	−68	−0.22
NIWA−UKCA	31,026	−68	−0.22
MRI	31,414	−70	−0.23
GEOSCCM	31,096	−67	−0.22
EMAC−L90	30,746	−72	−0.24
EMAC−L47	30,827	−73	−0.24
CMAM	31,359	−75	−0.24
CCSR/NIES	30,795	−66	−0.22
ACCESS	31,081	−69	−0.23
MMM	**31,022**	**−70**	**−0.23**
σ(MMM)	210	4	0.01

Note: Rounding can lead to seemingly wrong calculated values.

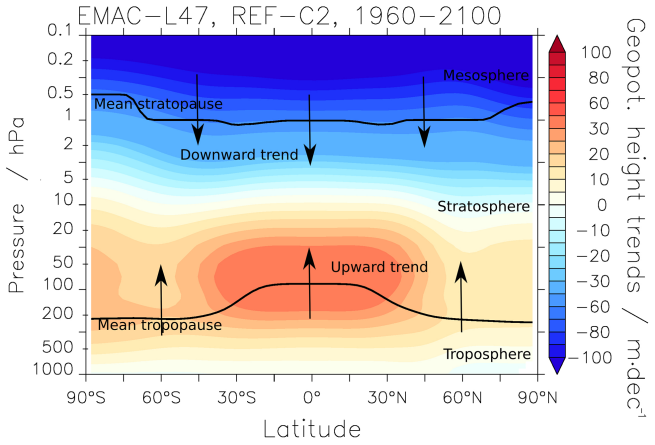

FIGURE 1 Zonal mean geopotential height trends (m·decade^{-1}) from the EMAC-L47 CCMI-1 REF-C2 simulation over the 1960–2100 period

Akmaev and Fomichev (1998) and Schmidt *et al.* (2006) have noted that in CO_2-doubling experiments, atmospheric changes can be very different for fixed height and fixed pressure. Berger and Lübken (2011) have shown that, due to the downward shift of pressure levels in the middle atmosphere, trends at geometric heights are larger than trends at pressure levels. For the BDC trends in the midlatitude lower stratosphere, this discrepancy has been quantified in Šácha *et al.* (2019) and a correction term has been proposed. Hence, the choice of the vertical coordinate significantly influences the statistical analysis of trends. In the following, we will show another mechanism by which trend estimates can be influenced by vertical structure changes of the atmosphere, even when the analysis is conducted on pressure levels – by the choice of log-pressure formulae. We show the impact on $\overline{w}^*$ trends, where the log-pressure formula is used for converting it from Pa·s^{-1} to m·s^{-1}.

The scale height H is defined as the height for which the atmospheric pressure decreases by a factor of e in an isothermal atmosphere. Generally, H depends on the temperature T and it can be calculated by

$$H = \frac{R\,T}{g}, \tag{2}$$

which can be derived from the barometric formula (assuming hydrostatic balance). Here, R is the gas constant 287.05 J·kg^{-1}·K^{-1}. For the stratosphere, H is commonly chosen to be 6950 m (e.g., the CCMI-1 data request; Hegglin *et al.*, 2015) to make the pressure levels resemble the geometric altitude. According to Equation (2), this corresponds to a stratospheric mean temperature of around 237.5 K, which is an arbitrary constant in the log-pressure system. However, when the stratosphere cools, the geometric (or geopotential) distance between pressure levels declines, according to the hypsometric equation (Equation (1)). In Equation (2), this process is reflected in the temperature dependence of the scale height and can be seen as a direct consequence of stratospheric cooling. The constant scale height assumption is commonly used in many well-established climate model diagnostics.

In the present study, we focus on the transformed Eulerian-mean (TEM) vertical velocity $\overline{w}^*$, which can be calculated by

$$\overline{w}^* = \overline{w} + \frac{\partial(\psi \cos\varphi)}{a \cos\varphi \, \partial\varphi}, \tag{3}$$

assuming hydrostatic balance (Andrews *et al.*, 1983). Here, a is the mean radius of the Earth, φ the latitude and $\psi = \overline{v'\theta'}/(\partial\overline{\theta}/\partial p)$. Andrews *et al.* (1987) and Hardiman *et al.* (2010) give details and the derivation of $\overline{w}^*$ for various approximations and coordinates. The overbar stands for the zonal mean. As most models use hybrid-pressure coordinates, the vertical velocity is usually available in $\mathrm{Pa \cdot s^{-1}}$ (then being denoted as ω) and is being converted to $\mathrm{m \cdot s^{-1}}$. For CCMI-1, Hegglin *et al.* (2015) implicitly recommend a log-pressure formula by defining a fixed scale height in their data request. The log-pressure definition of $\overline{w}^*$ is

$$\overline{w}^* = \overline{w} + \frac{1}{a \cos\varphi}\left(\cos\varphi \frac{\overline{v'\theta'}}{\partial\overline{\theta}/\partial\tilde{z}}\right), \tag{4}$$

where $\tilde{z}$ is the log-pressure height (Hardiman *et al.*, 2014, equation 23). In Equation (4), a conversion of vertical velocity and vertical derivative in pressure coordinates is assumed:

$$\overline{w} = -\frac{H}{p}\overline{\omega} \quad \text{and} \quad \partial\tilde{z} = -\frac{H}{p}\partial p. \tag{5}$$

This is identical to computing $\overline{\omega}^*$ using Equation (3) and making the transformation afterwards (note that the averaging is made on pressure levels) with

$$\overline{w}^* = -\frac{H}{p}\overline{\omega}^*. \tag{6}$$

The log-pressure formula has also been requested by the previous inter-model comparison activities CCMVal and CCMVal2 (Chemistry–Climate Model Validation Activity; SPARC, 2010). In the CCMVal data request, equation 3.5.1 of Andrews *et al.* (1987) (which here is Equation (4)) is explicitly asked for. However, using the general definition of the scale height (Equation (2)), the more general transformation

$$\overline{w}^* = -\frac{R\,\overline{T}}{p\,g}\overline{\omega}^* - \frac{R}{p\,g}\overline{T'\omega'} \tag{7}$$

emerges, which includes the temperature dependence and leads to the geopotential height vertical coordinate. At a leading order, the second term on the right-hand side can be neglected ($\mathcal{O}(\alpha^2)$), assuming small amplitudes of disturbances α. This is indeed the case in our test calculations with EMAC-L90; in the tropical upwelling region, this eddy term and also its trend are two orders of magnitude smaller than the first term with $\overline{T}$ dependence. For the lack of three-dimensional data of ω in the BADC repository, the term is neglected further in the study for the transformation between log-pressure and geopotential $\overline{w}^*$; that is, the following formula is used:

$$\overline{w}^* = -\frac{R\,\overline{T}}{p\,g}\overline{\omega}^*. \tag{8}$$

Dietmüller *et al.* (2018) have already noted in their supplement, that the CCMI-1 $\overline{w}^*$ of the EMAC-L90, EMAC-L47, SOCOLv3 and NIWA/UKCA models on the BADC (British Atmospheric Data Centre) server was uploaded using Equation (8) despite the conflict with the CCMI-1 data request, that is, not using the log-pressure formula. In fact, the Unified Model-based models NIWA/UKCA and ACCESS use hybrid-height as the native vertical coordinate and have a non-hydrostatic dynamical core, leading to the $\overline{w}^*$ calculation in $\mathrm{m \cdot s^{-1}}$ (Morgenstern *et al.*, 2009; 2013; Stone *et al.*, 2016). We assume that the models use equations 10 and 12 from Hardiman *et al.* (2010) to be accurate for non-hydrostatic and geometric coordinates. Climatologically, Dietmüller *et al.* (2018) quantified the effect of these different formulae to a $\overline{w}^*$ difference of 17% at 70 hPa for the EMAC-L90 REF-C1 simulation. For their multi-model analysis of CCMI-1 models, they recalculated log-pressure $\overline{w}^*$ from the given $\overline{v}^*$ fields using the continuity equation in log-pressure coordinate version for all models. Moreover, they encouraged anyone working with residual mean velocities from multi-model comparison projects to check if $\overline{w}^*$ is consistently calculated by comparison to the $\overline{v}^*$-derived $\overline{w}^*$ and, if necessary, to use those values for quantitative model comparisons. Besides this, Chrysanthou *et al.* (2019) stated that the TEM output from EMAC and SOCOLv3 was also calculated in conflict with the CCMI-1 data request using a temperature-dependent density and hence pointing to the geopotential height vertical coordinate. For CMIP5 (Coupled Model Intercomparison Project phase 5; Taylor *et al.*, 2012), $\overline{w}^*$ was not explicitly requested from the modelling groups. Studies like Manzini *et al.* (2014) that analysed $\overline{w}^*$ from CMIP5 model simulations asked the groups to compute it. Manzini *et al.* (2014) do not state which formula had been applied; it may have been chosen by individual groups, implying possible inconsistencies.

The literature has so far not appreciated that Equation (6) implicitly neglects the scale height changes due to stratospheric cooling. To quantify the error in trend calculations that arises due to increasing difference between distances in log-pressure and geometric coordinates (the relation between geometric and geopotential

coordinates is constant), we here calculate two different $\overline{w}^*$ trends for each CCMI-1 model. For models of the groups (MRI, GEOSCCM, CMAM, CCSR/NIES, ACCESS and WACCM) that delivered to the BADC server $\overline{w}^*$ transformed according to the log-pressure formula (Equation (6), in the following called $\overline{w}^*_H$), we calculate the temperature-dependent $\overline{w}^*$ (in the following called $\overline{w}^*_T$) for each latitude (ϕ) using Equations (6) and (8) as

$$\overline{w}^*_T(t,p,\phi) = \overline{w}^*_H(t,p,\phi)\frac{R\ \overline{T}(t,p,\phi)}{H\ g} \tag{9}$$

with $H = 6950$ m, dependent on time (t) and pressure level (p). For EMAC-L90, EMAC-L47 and SOCOLv3 which used Equation (8) for the transformation, we calculate the log-pressure version by

$$\overline{w}^*_H(t,p,\phi) = \overline{w}^*_T(t,p,\phi)\frac{H\ g}{R\ \overline{T}(t,p,\phi)} \tag{10}$$

to receive two different $\overline{w}^*$ estimates for each simulation. We also treat ACCESS and NIWA/UKCA as the models in the latter group, because the $\overline{w}^*$ from these two models is in geometric metres with a constant link to geopotential metres and thus reflects the temperature dependence. The difference between general non-hydrostatic TEM quantities and their hydrostatic analogues has been found to be negligibly small by Hardiman *et al.* (2010). The difference of the two respective $\overline{w}^*$ trends of each model yields an estimate of the implicitly neglected stratospheric cooling effect on the $\overline{w}^*_H$ trends (Equation (1)). Since we only quantify the trends in particular levels in this study, the reduced vertical resolution of the CCMI-1 data to 31 levels in the vertical does not significantly affect our results.

4 | ANALYSIS

4.1 | Trends of the residual vertical velocity $\overline{w}^*$

The strength of the advective part of the BDC is often diagnosed by means of $\overline{w}^*$ (e.g., Butchart *et al.*, 2010; Abalos *et al.*, 2015; Dietmüller *et al.*, 2018). Therefore, the estimate of the BDC acceleration in climate projections is biased through neglect of the decreasing scale height in the stratosphere. A number of studies have calculated $\overline{w}^*$ trends from the log-pressure version or from multi-model datasets and so can be affected (e.g., Garcia and Randel, 2008; Butchart *et al.*, 2010; Palmeiro *et al.*, 2014). The MMM tropical $\overline{w}^*$ trend difference profile is shown in Figure 2. The term 'tropical' stands for the mean value between the model-specific turnaround latitudes, which are for each month computed as the latitudes where $\overline{w}^*$ is zero. The trends were computed by a linear regression analysis of the 1960–2100 annual mean $\overline{w}^*$ values. The individual model trends as well as the differences for each individual model are provided in Figures S1 and S2.

The $\overline{w}^*_H$ trends are systematically larger than the $\overline{w}^*_T$ trends throughout the stratosphere. This could be expected, because the stratosphere cools in transient climate simulations from 1960 to 2100 and this influences the conversion equations (Equations (9) and (10)). To put this into perspective, the difference between the two $\overline{w}^*$ trends can be boiled down to the fact that the units of the vertical velocities are different although they are written identically: $\overline{w}^*_T$ is in geopotential m·s^{-1}, while $\overline{w}^*_H$ is in log-pressure m·s^{-1}.

Most models show a minimum of the absolute $\overline{w}^*$ differences in the middle stratosphere. The model spread of the $\overline{w}^*$ trend differences also shows a minimum in the middle stratosphere. However, the relative differences increase with altitude up to the upper stratosphere and also the model spread of the relative differences grows with altitude. This is mainly due to the small $\overline{w}^*_H$ trends in the middle stratosphere (Figure S1). The systematic difference between the two $\overline{w}^*$ trends clearly demonstrates that the oversimplified assumption of a constant scale height leads to an artificially enhanced $\overline{w}^*$ trend and thus to an overestimated acceleration of the advective BDC part.

As the stratosphere cools, the geopotential height difference (and the distance in geometric metres) between pressure levels decreases, but remains constant for log-pressure metres (equations 1.1.7 and 1.1.8 in Andrews *et al.*, 1987). Therefore, log-pressure metres are decreasing because geometric and geopotential metres are constant measures of distance. In other words, the original vertical velocity (in Pa·s^{-1}) increases in absolute values, even if the velocity in geometric (or geopotential in our case) m·s^{-1} is constant.

A widely used proxy for the strength of the advective BDC is the $\overline{w}^*$ value at 70 hPa (e.g., Hardiman *et al.*, 2014; Butchart *et al.*, 2010; Abalos *et al.*, 2015; Dietmüller *et al.*, 2018). Table 2 explicitly shows the $\overline{w}^*$ trends at 70 hPa of the eleven model simulations and the absolute and percentage differences between $\overline{w}^*_H$ and $\overline{w}^*_T$. The MMM of the above and its standard deviation are also shown.

The MMM of the $\overline{w}^*_H$ trend is 0.0047 mm·s^{-1}·decade^{-1} and of $\overline{w}^*_T$ it is 0.0038 mm·s^{-1}·decade^{-1}. Both trend estimates have an inter-model standard deviation of around 40% (not shown explicitly). The absolute differences between the two $\overline{w}^*$ trend estimates range between 0.0005 (GEOSCCM and ULAQ) and 0.0017 mm·s^{-1}·decade^{-1} (EMAC-L47). Despite this relatively large range in absolute trend differences, the differences in percentage have an inter-model standard deviation of only 2.9%. The MMM

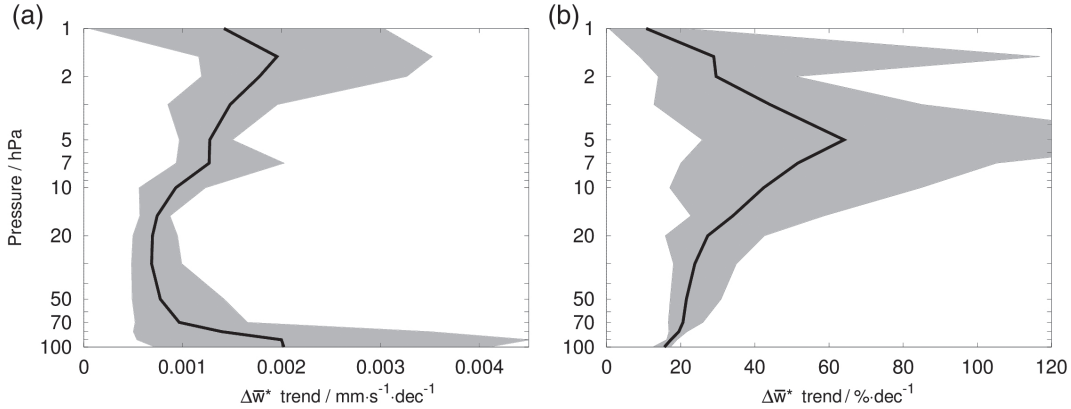

FIGURE 2 (a) Absolute and (b) relative multi-model mean differences of the tropical $\overline{w}^*$ trend estimates over the period 1960–2100 for the CCMI-1 REF-C2 simulations. The grey regions show the maximum and minimum of the model range. The absolute $\overline{w}^*$ difference is $\Delta\overline{w}^* = \overline{w}^*_H - \overline{w}^*_T$ and the relative $\overline{w}^*$ difference is $\Delta\overline{w}^* = (\overline{w}^*_H - \overline{w}^*_T)/\overline{w}^*_H$

TABLE 2 Overview of the linear trends of the two $\overline{w}^*$ calculations at 70 hPa within the turnaround latitudes of the CCMI-1 REF-C2 model simulations over the 1960–2100 period including MMM and the inter-model standard deviation (σ). All trends are significant on the 95% level. Figure S3 shows the time series of both $\overline{w}^*$ estimates. The absolute $\overline{w}^*$ difference is $\Delta\overline{w}^* = \overline{w}^*_H - \overline{w}^*_T$ and the relative $\overline{w}^*$ difference is $\Delta\overline{w}^* = (\overline{w}^*_H - \overline{w}^*_T)/\overline{w}^*_H$.

Model	$\overline{w}^*_H$ trend ($mm \cdot s^{-1} \cdot decade^{-1}$)	$\overline{w}^*_T$ trend ($mm \cdot s^{-1} \cdot decade^{-1}$)	$\Delta\overline{w}^*$ trend ($mm \cdot s^{-1} \cdot decade^{-1}$)	$\Delta\overline{w}^*$ trend (%)
WACCM	0.0028	0.0022	0.0006	20.7
ULAQ	0.0021	0.0016	0.0005	26.0
SOCOLv3	0.0043	0.0033	0.0011	24.8
NIWA	0.0077	0.0063	0.0013	17.0
MRI	0.0038	0.0030	0.0008	20.1
GEOSCCM	0.0027	0.0022	0.0005	19.3
EMAC-L90	0.0072	0.0055	0.0016	22.4
EMAC-L47	0.0078	0.0061	0.0017	21.2
CMAM	0.0048	0.0038	0.0010	21.4
CCSR/NIES	0.0053	0.0043	0.0009	17.4
ACCESS	0.0038	0.0032	0.0006	16.7
MMM	**0.0047**	**0.0038**	**0.0010**	**20.7**
σ(MMM)	0.0019	0.0016	0.0004	2.9

Note. That rounding can lead to seemingly wrong values.

of the trend difference is 20.7%, and so the uncertainty in percentage is only around 14% of the MMM. Therefore, at 70 hPa the relative change is more consistent among the models than the absolute change; this can also be seen in Figure 2. To assess if the uncertainty connected with the determination of the turnaround latitudes has an impact on our results, we have also performed the calculations between fixed latitudes (20°S–20°N), yielding similar results; the MMM relative difference is 19.9% and its standard deviation 1.8%. Overall, this means that, when estimated using the $\overline{w}^*_H$ trend at 70 hPa, around 20% of the advective BDC acceleration in climate projection simulations is artificial, that is, due to neglecting stratospheric cooling.

The same values as in Table 2, but for 10 hPa, are provided in Table S1. The $\overline{w}^*$ relative differences at 10 hPa are generally larger than at 70 hPa, the MMM of $\Delta\overline{w}^*$ (10 hPa) is 42.9%. However, that is mainly due to the fact that in general the $\overline{w}^*$ trends are much lower there (Figure S1). Some of the $\overline{w}^*$ trends at 10 hPa are not even significant (Table S1). The model spread at 10 hPa is much larger (17.3%) than at 70 hPa (2.9%). This is mainly due

to the general decrease of the $\overline{w}^*$ trend with altitude, which appears in the denominator when calculating the percentage difference.

4.2 | Effect on residual streamfunction and mass flux

The residual mean streamfunction and the tropical upward mass flux, which are defined using $\overline{w}^*$, are among the other quantities that are widely used to study stratospheric transport. The residual mean streamfunction is calculated as

$$\psi^*(\phi) = \int 2\pi a^2 \cos(\phi)\, \overline{\rho w}^*\, \mathrm{d}\phi, \tag{11}$$

with a being the mean Earth's radius, ϕ the latitude and $\overline{\rho}$ the density. Depending on the vertical coordinate system, $\overline{\rho}$ can either be computed using a constant scale height in the log-pressure system:

$$\overline{\rho}_c = \overline{\rho}_0 \exp\left(-\frac{\tilde{z}}{H}\right) = \frac{p}{g\,H} \tag{12}$$

(with $\overline{\rho}_0 = p_0/(R\overline{T}_0)$ and $\tilde{z}$ being the log-pressure height), or using the ideal gas law for dry air:

$$\overline{\rho}_T(T) = \frac{p}{R\,\overline{T}}. \tag{13}$$

The scaling of $\overline{w}^*$ with $\overline{\rho}$ to calculate the streamfunction (Equation (11)) can either be done with the constant scale height assumption for both $\overline{w}^*$ and $\overline{\rho}$, that is, using the log-pressure formula, by

$$\overline{w}^*_H \rho_c = \overline{\omega}^* \frac{H}{-p}\frac{p}{gH} = \overline{\omega}^* \left(\frac{1}{-g}\right) \tag{14}$$

to yield ψ^*_{Hc}, or using the geopotential conversion, that is, dependent on temperature for both $\overline{w}^*$ and $\overline{\rho}$, by

$$\overline{w}^*_T(\overline{T})\rho_T(T) = \overline{\omega}^* \frac{R\overline{T}}{-pg}\frac{p}{R\overline{T}} = \overline{\omega}^* \left(\frac{1}{-g}\right), \tag{15}$$

to yield ψ^*_{TT}. As it could have been expected, the two formulae yield identical results, because the density trend dependence cancels the $\overline{w}^*$ trend dependence on the vertical coordinate. On a more general note, the cancellation can be inferred directly from dimensional analysis, because streamfunction (and mass flux) has the unit $\mathrm{kg{\cdot}s^{-1}}$ and is therefore insensitive to the vertical coordinate. Only quantities that include metres (in the vertical direction) in their units can be affected.

However, inconsistent usage of Equation (11) can lead to streamfunction trend (and climatology) differences. In particular, scaling $\overline{w}^*_H$ with $\overline{\rho}_T$ would yield

$$\psi^*_{HT}(\phi) = \int 2\pi a^2 \cos(\phi)\, \overline{\rho}_T\, \overline{w}^*_H\, \mathrm{d}\phi, \tag{16}$$

and scaling $\overline{w}^*_T$ with $\overline{\rho}_c$ yields

$$\psi^*_{Tc}(\phi) = \int 2\pi a^2 \cos(\phi)\, \overline{\rho}_c\, \overline{w}^*_T\, \mathrm{d}\phi. \tag{17}$$

To provide an estimate for that error, Figure 3 shows the MMM ψ^* trend differences ($\Delta\psi^*_{Tc-TT}$ and $\Delta\psi^*_{HT-TT}$) which emerge from this kind of inconsistent calculation of the streamfunction for the eleven CCMI-1 REF-C2 simulations.

Figure 3 shows a considerable overestimation of the streamfunction trend if $\overline{w}^*_H$ is used and an underestimation if the constant $\overline{\rho}_c$ is used. Again, this is a direct consequence of stratospheric cooling and could be expected from the equations above. Particularly in the lower stratosphere, the trend differences are comparatively large. Next, this will be quantified more precisely by means of calculating the tropical upward mass flux trends.

The tropical upward mass flux can be computed directly from the streamfunction by

$$F(p,\phi) = \max\{\psi^*(p,\phi)\} - \min\{\psi^*(p,\phi)\} \tag{18}$$

for each pressure level and latitude. Hence, the same facts which apply to the streamfunction also apply to the mass flux: consistent usage of the assumptions (F_{TT} and F_{Hc}) leads to the cancellation of the effect ($\Rightarrow F_{TT} = F_{Hc}$), but inconsistent usage (F_{HT} and F_{Tc}) leads to trend (and climatology) differences. Figure 4 shows the multi-model mean trend differences of the mass flux estimates as a function of altitude with the absolute and relative values. All three estimates of the absolute mass flux trends of each model individually are provided in Figure S5.

The F_{HT} trend is larger than the F_{TT} ($= F_{Hc}$) trend throughout the stratosphere and the F_{Tc} trend is smaller. In absolute values, the trend difference decreases strongly with altitude because mass flux generally is much smaller in the upper stratosphere. The relative values range between 15 and 35% and −15 and −35%, respectively, with a maximum in the upper stratosphere. There, the range between maxima and minima is very large, because the CMAM model simulates downward mass fluxes, which is consistent with the negative vertical velocities detected in CMAM. At 70 hPa (the traditional pressure level for mass flux analysis, e.g., Butchart *et al.*, 2010), the MMM of the mass flux trend differences are 28.5% for F_{HT} and −21.5% for F_{Tc} (Figure S6 and Table S2).

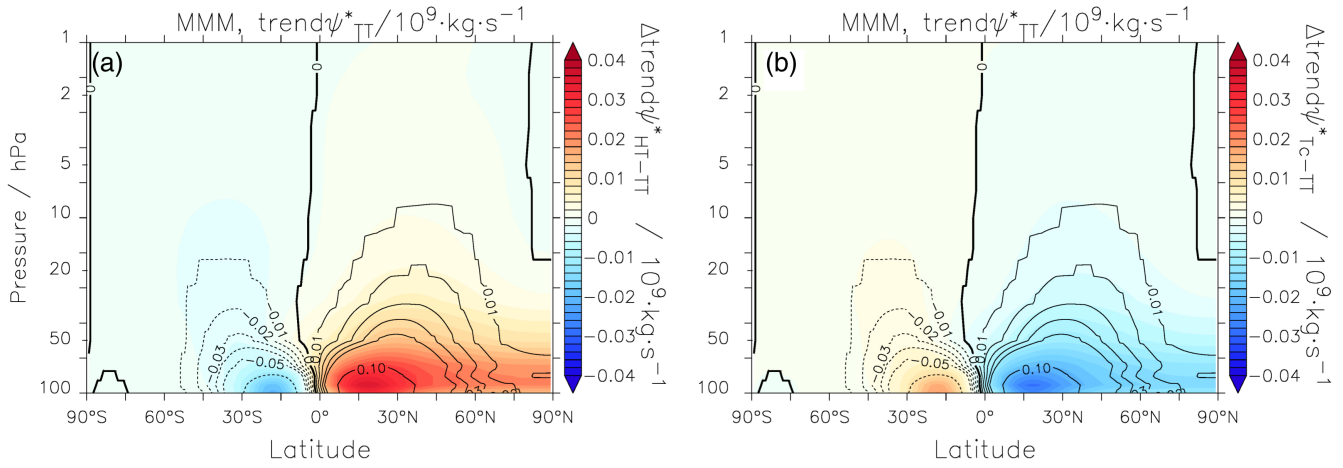

FIGURE 3 Trend differences (colour shading) of the residual streamfunctions as calculated inconsistently with (a) $\overline{w}^*_H$ and $\overline{\rho}_T$ and (b) $\overline{w}^*_T$ and $\overline{\rho}_c$, both minus the reference streamfunction $\psi^*_{TT} = \psi^*_{Hc}$. The contour lines show the ψ^*_{TT} for reference

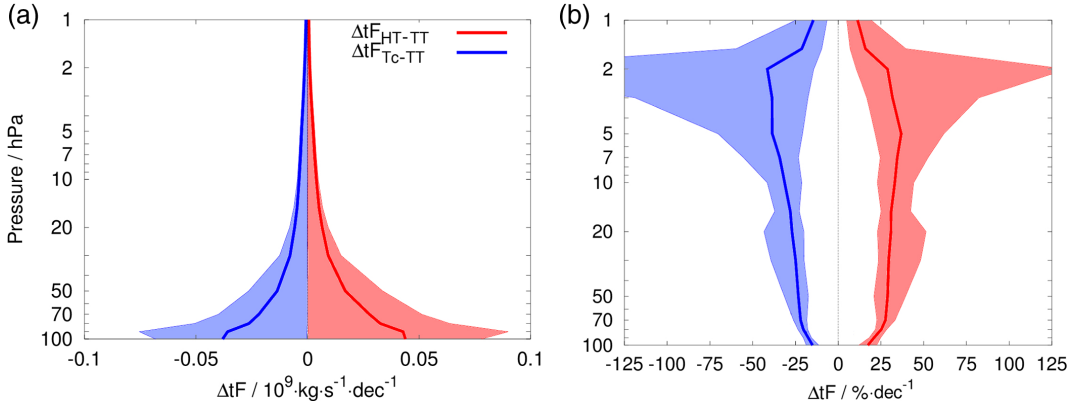

FIGURE 4 MMM trend differences of the tropical upward mass flux as calculated inconsistently with $\overline{w}^*_H$ and $\overline{\rho}_T$ (yielding F_{HT}) and $\overline{w}^*_T$ and $\overline{\rho}_c$ (yielding F_{Tc}) as (a) absolute and (b) relative values. The shaded regions show the maxima and minima of the models. The absolute trend (t) differences are $tF_{HT} - tF_{TT}$ and $tF_{Tc} - tF_{TT}$ and the relative differences are $100(tF_{HT} - tF_{TT})/tF_{TT}$ and $100(tF_{Tc} - tF_{TT})/tF_{TT}$

In summary, the density trends cancel out the temperature dependence of $\overline{w}^*$, however this applies only if the conversion equations are chosen consistently for both $\overline{w}^*$ and ρ. Inconsistent usage leads to considerable errors in the mass flux and streamfunction trend estimates. It is important always to be aware of which particular $\overline{w}^*$ and ρ are analysed.

5 | DISCUSSION

While tropospheric warming leads to an expansion of the troposphere (Vallis *et al.*, 2015; Oberländer-Hayn *et al.*, 2016; Abalos *et al.*, 2017), stratospheric cooling contracts the pressure levels in the stratosphere (Šácha *et al.*, 2019). Across the period 1960–2100, the CCMI-1 models simulate that the distance between 100 and 1 hPa shrinks by about 70 m·decade^{-1}. This is around 0.2%·decade^{-1} of the climatological distance and is consistent among the eleven analysed model simulations. Berger and Lübken (2011) and Šácha *et al.* (2019) have shown that, due to the vertical shift of pressure levels, trends computed in geopotential (or geometric) coordinates are different from trends computed in pressure levels. In the present paper we point out another trivial consequence – that in the stratosphere, the reduction of pressure level distances causes a decrease of the scale height H. However, for various dynamical diagnostics, the common calculation (or conversion) method includes a constant H. One prominent diagnostic of this type is the residual vertical velocity $\overline{w}^*$. For the CCMI-1 data request, Hegglin *et al.* (2015) suggest the log-pressure formula including the constant scale height 6950,m for computation of $\overline{w}^*$.

We compare the trends of stratospheric $\overline{w}^*$ in the Tropics (within the turnaround latitudes) as converted with the suggested log-pressure formula with constant H

($\overline{w}^*_H$) and with a more general conversion method which includes the temperature dependence ($\overline{w}^*_T$). Dietmüller *et al.* (2018) have already shown that at 70 hPa, the climatological value of $\overline{w}^*_H$ is about 17% larger than that of $\overline{w}^*_T$. Our analysis shows that also the trend of $\overline{w}^*_H$ is systematically larger than that of $\overline{w}^*_T$ throughout the stratosphere in all eleven analysed CCMI-1 simulations. The $\overline{w}^*$ differences show a minimum in the middle stratosphere; this is also where the trend values are smallest, hence the relative differences grow with altitude. At 70 hPa, the two $\overline{w}^*$ trend estimates differ by 20.7% in the multi-model mean, with an inter-model standard deviation of only 2.9%, showing consistency among the models. At 10 hPa, the percentage differences are generally larger (42.9%), but also the model spread is much larger (17.3%) and the trends are partly not significant. Via the hypsometric equation, the direct cause of the $\overline{w}^*$ trend differences is the local temperature trend. The pressure level shift is directly induced by the local temperature trend and scale height changes. Note that this pressure level contraction should not be mistaken for the distance reduction between tropopause and stratopause. The stratospheric contraction as diagnosed by the distance between the tropopause and stratopause can additionally be influenced by pressure changes at these levels, but this does not have an effect on the scale height. However, it can have an influence on the BDC in a yet unquantified manner.

A number of studies have calculated $\overline{w}^*$ trends (or trends of diagnostics that are based on $\overline{w}^*$) for climate change simulations using log-pressure formulae (e.g., Garcia and Randel, 2008; Butchart *et al.*, 2010; Palmeiro *et al.*, 2014). The difference in the two $\overline{w}^*$ trend estimates can have consequences for research on stratospheric dynamics. Based on our results, we estimate that BDC trends that are based on $\overline{w}^*$ can be overestimated by about 20%. However, in order to quantitatively understand climate change-induced trends, they have to be computed as accurately as possible, otherwise studies that for example attribute stratospheric tracer trends to changes in upward transport may be biased. The difference will presumably be multiplicative, that is, for example, a 40% contribution of upward velocities to tropical lower stratospheric ozone trends would bear an 8% error in ozone trend contribution.

Not only the $\overline{w}^*$ trends are affected by the constant scale height assumption, which is implicit to the log-pressure formulae. The widely used Eliassen–Palm (EP) flux diagnostic in log-pressure form (Andrews *et al.*, 1987) uses $\hat{F}(z) = -(H/p_0)F(p)$ for conversion of the vertical component of the EP flux $\hat{F}(z)$ or $F(p)$ in the CMIP6 DynVarMIP data request (Gerber and Manzini, 2016). Therefore, trend analyses of this quantity can also be biased by the effect of stratospheric cooling (also Hardiman *et al.*, 2010). However, the magnitude of the error in trend analyses with this or other quantities must be evaluated for every individual case.

The streamfunction and the tropical upward mass flux are not affected by the error in $\overline{w}^*$, because the density trend and the scale height trend cancel each other out. In a general perspective, only diagnostics with units including metres can be affected because these can be sensitive to the variable relationship between log-pressure and geometric metres. Note, however, that horizontal distances are not affected by the constant scale height assumption. Still, care has to be taken because, if the scaling for the streamfunction and mass flux calculations is done inconsistently (i.e., if a constant density is mixed with $\overline{w}^*_T$, or a temperature-dependent density with $\overline{w}^*_H$), errors in the streamfunction or mass flux trend can occur also. And it is fairly easy to make this mistake, because for the CCMI data repository, some modelling groups delivered $\overline{w}^*$ computed other than with the log-pressure formula, despite the request to use the log-pressure formula. Moreover, in most papers, the exact conversion method from $\mathrm{Pa{\cdot}s^{-1}}$ to $\mathrm{m{\cdot}s^{-1}}$ is not provided. This can also make it impossible to conclusively estimate the errors that may have been made in past studies without direct contact with the respective researchers. In the case of the mass flux trends, our estimation of the possible error is either almost 30% or around −20%, respectively for the two error sources.

We have analysed $\overline{w}^*$ data of the CCMI-1 simulations, however, the log-pressure formula for conversion can be found in most of the data requests in multi-model comparison projects. The CCMVal and CCMVal-2 (SPARC, 2010) and the CMIP6 (Eyring *et al.*, 2016) DynVarMIP (Gerber and Manzini, 2016) data requests also include the formula. In CMIP5 (Taylor *et al.*, 2012) $\overline{w}^*$ was not explicitly provided, but there are still studies that analysed $\overline{w}^*$ from CMIP5 simulations. For example, Manzini *et al.* (2014) used $\overline{w}^*$ data computed by the modelling centres, and in that case it is not possible to track which conversion equations have been applied and so an error estimation is hardly feasible. Also for the first stratospheric multi-model assessments of chemistry climate models (Austin *et al.*, 2003), a clear documentation of equation usage could not be found. Furthermore, the log-pressure equations with constant scale height are generally common and widely used by operators of climate data processing algorithms. Our results strongly recommend that use of a constant scale height for computing diagnostics should be avoided in climate change simulations. In particular, we call on multi-climate-model projects to consider the effect of varying geopotential height of pressure levels in their data requests. For example, for CCMI-2 it is not too late to tell the modelling centres to avoid formulae with the constant scale height assumption. Similar effects of opposite sign

can also be generally expected in the troposphere which is thermally expanding.

6 | CONCLUSIONS

Stratospheric cooling leads to decreasing distances between pressure levels in the stratosphere. In the course of current climate change, the distance between 100 and 1 hPa is decreasing by about 70 m per decade. The stratospheric scale height decreases as a consequence of the contraction of pressure levels. However, a constant scale height is assumed in the CCMI-1 data request for computation of the residual mean vertical velocity $\overline{w}^*$ in the log-pressure form (Hegglin *et al.*, 2015), a diagnostic that is often used as a proxy for the advective Brewer–Dobson circulation (BDC) strength. Analysing eleven CCMI-1 REF-C2 simulations over the period 1960–2100, our study shows that the constant scale height assumption leads to a ∼20% overestimation of the $\overline{w}^*$ trends. In this diagnostic framework, stratospheric cooling therefore leads to an overestimation of the advective BDC acceleration. Other diagnostics like the vertical EP flux are also affected by the error. For the streamfunction as well as the upward mass flux, the computation has to be done consistently with the definition to avoid inaccuracies in their trends, a mistake that can easily be committed because details of the transformation are often unknown. For the data of other multi-model projects and also for individually processed data, the same log-pressure formulae have been used (e.g., SPARC, 2010; Gerber and Manzini, 2016, for CCMVal and CMIP6, respectively). Our study calls for caution when making trend analyses of dynamic or transport variables as the relationships between coordinate systems can alter through climate change. For $\overline{w}^*$, one should keep in mind that previous studies may bear a 20% error in their trend calculations, thereby overestimating the advective BDC acceleration. This also implies that the contribution estimate of stratospheric tracer trends to the BDC acceleration may be incorrect. In the long run, we encourage those responsible to change their data processing tools and especially to reformulate data requests regarding multi-model assessments.

ACKNOWLEDGEMENTS

RE is funded by the Helmholtz Association under grant VH-NG-1014 (Helmholtz-Hochschul-Nachwuchsforschergruppe MACClim). PS is supported through the project CZ.02.2.69/0.0/0.0/19_074/0016231 (International mobility of researchers at Charles University (MSCA-IF III)) for the research stay at BOKU Vienna, through the ED481B 2018/103 grant of the Xunta de Galicia, the Czech ScienceFoundation (GAČR) under grant nos.16-01562J and 18-01625S and acknowledges discussions in the New Quantitative Constraints on OGW Stress and Drag team at the International Space Science Institute in Bern, Switzerland. We also acknowledge funding from the Bayerisch-Tschechische Hochschulagentur (BTHA/BAYHOST) under grant number BTHA-MOB-2020-2. Moreover, we thank Petr Pišoft, Hella Garny, Harald Rieder, Patrick Jöckel, Robert Sausen, and Martin Dameris for discussions, Olaf Morgenstern, Laura Revell, Rolando Garcia, Hideharu Akiyoshi and Markus Rapp for comments on the manuscript, and Martin Dameris (again) as well as two anonymous referees for reviewing the paper.

We thank the modelling groups for making their simulations available for this analysis, the SPARC/IGAC Chemistry–Climate Model Initiative (CCMI) project for organising and coordinating the model data analysis activity and the British Atmospheric Data Centre (BADC) for collecting and archiving the CCMI model output. The ACCESS-CCM simulations were supported by the Australian Research Council's Centre of Excellence for Climate System Science (CE110001028), the Australian Government's National Computational Merit Allocation Scheme (q90) and the Australian Antarctic science grant programme (FoRCES 4012). The CCSR/NIES simulations were performed on NEC-SX9/A(ECO) and NEC-SXACE computers at the Center for Global Environmental Research (CGER), National Institute for Environmental Studies (NIES), and supported by the Environment Research and Technology Development Fund, Ministry of Environment, Japan (2-1303 and 2-1709). The EMAC simulations were conducted at the German Climate Computing Centre DKRZ through support from the Bundesministerium für Bildung und Forschung (BMBF) within the project ESCiMo (Earth System Chemistry integrated Modelling). For the WACCM results, computing resources (ark:/85065/d7wd3xhc) were provided by the Climate Simulation Laboratory at NCAR's Computational and Information Systems Laboratory, sponsored by the National Science Foundation and other agencies. The MetUM was developed by the UK Met Office. The NIWA simulations were carried out within the program CACV by the NZ Governments Strategic Science Investment Fund (SSIF) with support from the New Zealand eScience Infrastructure (NeSI), which is funded by NeSIs collaborator institutions and through the Ministry of Business, Innovation & Employments Research Infrastructure programme.

DATA AVAILABILITY

All CCMI-1 data used in this study can be obtained through the British Atmospheric Data Centre (BADC) archive (ftp://ftp.ceda.ac.uk; accessed 1 February 2020). CESM1-WACCM data have been downloaded from

http://www.earthsystemgrid.org (last access: 1 February 2020).

ORCID

Roland Eichinger https://orcid.org/0000-0001-6872-5700
Petr Šácha https://orcid.org/0000-0001-9707-1750

REFERENCES

Abalos, M., Legras, B., Ploeger, F. and Randel, W.J. (2015) Evaluating the advective Brewer–Dobson circulation in three reanalyses for the period 1979–2012. *Journal of Geophysical Research: Atmospheres*, 120, 7534–7554. https://doi.org/10.1002/2015JD023182

Abalos, M., Randel, W.J., Kinnison, D.E. and Garcia, R.R. (2017) Using the artificial tracer e90 to examine present and future UTLS tracer transport in WACCM. *Journal of the Atmospheric Sciences*, 74, 3383–3403. https://doi.org/10.1175/JAS-D-17-0135.1

Akiyoshi, H., Nakamura, T., Miyasaka, T., Shiotani, M. and Suzuki, M. (2016) A nudged chemistry–climate model simulation of chemical constituent distribution at northern high-latitude stratosphere observed by SMILES and MLS during the 2009/2010 stratospheric sudden warming. *Journal of Geophysical Research: Atmospheres*, 121, 1361–1380. https://doi.org/10.1002/2015JD023334

Akmaev, R.A. and Fomichev, V.I. (1998) Cooling of the mesosphere and lower thermosphere due to doubling of CO_2. *Annales Geophysicae*, 16, 1501–1512. https://doi.org/10.1007/s00585-998-1501-z

Andrews, D.G., Mahlman, J.D. and Sinclair, R.W. (1983) Eliassen–Palm diagnostics of wave–mean flow interaction in the GFDL "SKYHI" general circulation model. *Journal of the Atmospheric Sciences*, 40, 2768–2784. https://doi.org/10.1175/1520-0469(1983)040<2768:ETWATM>2.0.CO;2

Andrews, D.G., Holton, J.R. and Leovy, C.B. (1987) *Middle Atmosphere Dynamics*. Academic Press, Cambridge, MA. https://books.google.de/books/about/Middle_Atmosphere_Dynamics.html?id=N1oNurYZefAC&source=kp_cover&redir_esc=y

Austin, J., Shindell, D., Beagley, S.R., Brühl, C., Dameris, M., Manzini, E., Nagashima, T., Newman, P., Pawson, S., Pitari, G., Rozanov, E., Schnadt, C. and Shepherd, T.G. (2003) Uncertainties and assessments of chemistry–climate models of the stratosphere. *Atmospheric Chemistry and Physics*, 3, 1–27. https://doi.org/10.5194/acp-3-1-2003

Austin, J., Wilson, R.J., Akiyoshi, H., Bekki, S., Butchart, N., Claud, C., Fomichev, V.I., Forster, P., Garcia, R.R., Gillett, N.P., Keckhut, P., Langematz, U., Manzini, E., Nagashima, T., Randel, W.J., Rozanov, E., Shibata, K., Shine, K.P., Struthers, H., Thompson, D.W.J., Wu, F. and Yoden, S. (2009) Coupled chemistry climate model simulations of stratospheric temperatures and their trends for the recent past. *Geophysical Research Letters*, 36. https://doi.org/10.1029/2009GL038462

Berger, U. and Lübken, F.-J. (2011) Mesospheric temperature trends at mid-latitudes in summer. *Geophysical Research Letters*, 38(L22 804). https://doi.org/10.1029/2011GL049528

Butchart, N., Cionni, I., Eyring, V., Shepherd, T., Waugh, D., Akiyoshi, H., Austin, J., Brühl, C., Chipperfield, M., Cordero, E., Dameris, M., Deckert, R., Dhomse, S., Frith, S.M., Garcia, R.R., Gettelman, A., Giorgetta, M.A., Kinnison, D.E., Li, F., Mancini, E., McLandress, C., Pawson, S., Pitari, G., Plummer, D.A., Rozanov, E., Sassi, F., Scinocca, J.F., Shibata, K., Steil, B. and Tian, W. (2010) Chemistry–climate model simulations of twentyfirst century stratospheric climate and circulation changes. *Journal of Climate*, 23, 5349–5374. https://doi.org/10.1175/2010JCLI3404.1

Chrysanthou, A., Maycock, A.C., Chipperfield, M.P., Dhomse, S., Garny, H., Kinnison, D., Akiyoshi, H., Deushi, M., Garcia, R.R., Jöckel, P., Kirner, O., Pitari, G., Plummer, D.A., Revell, L., Rozanov, E., Stenke, A., Tanaka, T.Y., Visioni, D. and Yamashita, Y. (2019) The effect of atmospheric nudging on the stratospheric residual circulation in chemistry–climate models. *Atmospheric Chemistry and Physics*, 19, 11 559–11 586. https://doi.org/10.5194/acp-19-11559-2019

Deushi, M. and Shibata, K. (2011) Development of a Meteorological Research Institute chemistry–climate model version 2 for the study of tropospheric and stratospheric chemistry. *Papers in Meteorology and Geophysics*, 62, 1–46. https://doi.org/10.2467/mripapers.62.1

Dietmüller, S., Eichinger, R., Garny, H., Birner, T., Boenisch, H., Pitari, G., Mancini, E., Visioni, D., Stenke, A., Revell, L., Rozanov, E., Plummer, D.A., Scinocca, J., Jöckel, P., Oman, L., Deushi, M., Kiyotaka, S., Kinnison, D.E., Garcia, R., Morgenstern, O., Zeng, G., Stone, K.A. and Schofield, R. (2018) Quantifying the effect of mixing on the mean age of air in CCMVal-2 and CCMI-1 models. *Atmospheric Chemistry and Physics Discussions*, 18, 1–34. https://doi.org/10.5194/acp-2017-1143

Eichinger, R., Dietmüller, S., Garny, H., Šácha, P., Birner, T., Böhnisch, H., Pitari, G., Visioni, D., Stenke, A., Rozanov, E., Revell, L., Plummer, D.A., Jöckel, P., Oman, L., Deushi, M., Kinnison, D.E., Garcia, R., Morgenstern, O., Zeng, G., Stone, K.A. and Schofield, R. (2019) The influence of mixing on the stratospheric age of air changes in the 21st century. *Atmospheric Chemistry and Physics*, 19, 921–940. https://doi.org/10.5194/acp-19-921-2019

Eyring, V., Lamarque, J.-F., Hess, P., Arfeuille, F., Bowman, K., Chipperfield, M., Duncan, B., Fiore, A., Gettelman, A., Gior-getta, M., Granier, C., Hegglin, M., Kinnison, D., Kunze, M., Langematz, U., Luo, B., Martin, R., Matthes, K., Newman, P., Peter, T., Robock, A., Ryerson, A., Saiz-Lopez, A., Salawitch, R., Schultz, M., Shepherd, T., Shindell, D., Stähelin, J., Tegt-meier, S., Thomason, L., Tilmes, S., Vernier, J.-P., Waugh, D. and Young, P. (2013) Overview of IGAC/SPARC Chemistry-Climate Model Initiative (CCMI) community simulations in support of upcoming Ozone and climate assessments. *SPARC Newsletter*, 40, 48–66.

Eyring, V., Bony, S., Meehl, G.A., Senior, C.A., Stevens, B., Stouffer, R.J. and Taylor, K.E. (2016) Overview of the coupled model intercomparison project phase 6 (CMIP6) experimental design and organization. *Geoscientific Model Development*, 9, 1937–1958. https://doi.org/10.5194/gmd-9-1937-2016

Fu, Q., Johanson, C.M., Warren, S.G. and Seidel, D.J. (2004) Contribution of stratospheric cooling to satellite-inferred tropospheric temperature trends. *Nature*, 429, 55–58. https://doi.org/10.1038/nature02524

Funatsu, B.M., Claud, C., Keckhut, P., Hauchecorne, A. and Leblanc, T. (2016) Regional and seasonal stratospheric temperature trends in the last decade (2002–2014) from AMSU observations. *Journal of Geophysical Research: Atmospheres*, 121, 8172–8185. https://doi.org/10.1002/2015JD024305

Garcia, R.R. and Randel, W.J. (2008) Acceleration of the Brewer–Dobson circulation due to increases in greenhouse gases.

Journal of the Atmospheric Sciences, 65, 2731–2739. https://doi.org/10.1175/2008JAS2712.1

Gerber, E.P. and Manzini, E. (2016) The dynamics and variability model intercomparison project (DynVarMIP) for CMIP6: assessing the stratosphere–troposphere system. *Geoscientific Model Development*, 9, 3413–3425. https://doi.org/10.5194/gmd-9-3413-2016

Gettelman, A., Hegglin, M.I., Son, S.-W., Kim, J., Fujiwara, M., Birner, T., Kremser, S., Rex, M., Añel, J.A., Akiyoshi, H., Austin, J., Bekki, S., Braesike, P., Brühl, C., Butchart, N., Chipperfield, M., Dameris, M., Dhomse, S., Garny, H., Hardiman, S.C., Jöckel, P., Kinnison, D.E., Lamarque, J.F., Mancini, E., Marchand, M., Michou, M., Morgenstern, O., Pawson, S., Pitari, G., Plummer, D., Pyle, J.A., Rozanov, E., Scinocca, J., Shepherd, T.G., Shibata, K., Smale, D., Teyssedre, H. and Tian, W. (2010) Multimodel assessment of the upper troposphere and lower stratosphere: tropics and global trends. *Journal of Geophysical Research*, 115, D00M08. https://doi.org/10.1029/2009JD013638

Granier, C., Bessagnet, B., Bond, T., D'Angiola, A., van der Gon, H.D., Frost, G.J., Heil, A., Kaiser, J.W. and Kinne, S. (2011) Evolution of anthropogenic and biomass burning emissions of air pollutants at global and regional scales during the 1980–2010 period. *Climate Change*, 109, 163–190. https://doi.org/10.1007/s10584-011-0154-1

Hardiman, S.C., Andrews, D.G., White, A.A., Butchart, N. and Edmond, I. (2010) Using different formulations of the transformed Eulerian mean equations and Eliassen–Palm diagnostics in general circulation models. *Journal of the Atmospheric Sciences*, 67, 1983–1995. https://doi.org/10.1175/2010JAS3355.1

Hardiman, S.C., Butchart, N. and Calvo, N. (2014) The morphology of the Brewer–Dobson circulation and its response to climate change in CMIP5 simulations. *Quarterly Journal of the Royal Meteorological Society*, 140, 1958–1965. https://doi.org/10.1002/qj.2258

Hegglin, M., Lamarque, J. and Eyring, V. (2015) *The IGAC/SPARC Chemistry-Climate Model Initiative Phase-1 (CCMI-1) model data output*. NCAS British Atmospheric Data Centre. http://catalogue.ceda.ac.uk/uuid/9cc6b94df0f4469d8066d69b5df879d5; accessed 28 July 2020.

Hegglin, M., Lamarque, J., Duncan, B., Eyring, V., Gettelman, A., Hess, P., Myhre, G., Nagashima, T., Plummer, D., Ryerson, T., Shepherd, T. and Waugh, D. (2016) Report on the IGAC/SPARC Chemistry-Climate Model Initiative (CCMI) 2015 Science Workshop. *SPARC Newsletter*, 46, 37–42.

Imai, K., Manago, N., Mitsuda, C., Naito, Y., Nishimoto, E., Sakazaki, T., Fujiwara, M., Froidevaux, L., von Clarmann, T., Stiller, G.P., Murtagh, D.P., Rong, P.-P., Mlynczak, M.G., Walker, K.A., Kinnison, D.E., Akiyoshi, H., Nakamura, T., Miyasaka, T., Nishibori, T., Mizobuchi, S., Kikuchi, K.-I., Ozeki, H., Takahashi, C., Hayashi, H., Sano, T., Suzuki, M., Takayanagi, M. and Shiotani, M. (2013) Validation of ozone data from the Superconducting Submillimeter-Wave Limb-Emission Sounder (SMILES). *Journal of Geophysical Research: Atmospheres*, 118, 5750–5769. https://doi.org/10.1002/jgrd.50434

IPCC (2013). Summary for Policymakers, in: Climate Change 2013: The Physical Science Basis, Contribution of Working Group I to the Fifth Assessment Report of the IPCC. Stocker, T.F., Qin, D., Plattner, G.K., Tignor, M., Allen, S.K., Boschung, J., Nauels, A., Xia, Y., Bex, V., Midgley, P.M. (eds), Cambridge University Press, Cambridge, UK.

Jacobi, C. (2014) Meteor heights during the recent solar minimum. *Advances in Radio Science*, 12, 161–165. https://doi.org/10.5194/ars-12-161-2014

Jöckel, P., Kerkweg, A., Pozzer, A., Sander, R., Tost, H., Riede, H., Baumgaertner, A., Gromov, S. and Kern, B. (2010) Development cycle 2 of the Modular Earth Submodel System (MESSy2). *Geoscientific Model Development*, 3, 717–752. https://doi.org/10.5194/gmd-3-717-2010

Jöckel, P., Holger, T.O., Pozzer, A., Kunze, M., Kirner, O., Brenninkmeijer, C., Brinkop, S., Cai, D., Dyroff, C., Eckstein, J., Frank, F., Garny, H., Gottschaldt, K.-D., Graf, P., Grewe, V., Kerkweg, A., Kern, B., Matthes, S., Mertens, M., Meul, S., Neumaier, M., Nützel, M., Oberländer-Hayn, S., Ruhnke, R., Runde, T., Sander, R., Scharffe, D. and Zahn, A. (2016) Earth System Chemistry Integrated Modelling (ESCiMO) with the Modular Earth Submodel System (MESSy, version 2.51). *Geoscientific Model Development*, 9, 1153–1200. https://doi.org/10.5194/gmd-9-1153-2016

Jonsson, A., De Grandpre, J., Fomichev, V., McConnell, J. and Beagley, S. (2004) Doubled CO2-induced cooling in the middle atmosphere: photochemical analysis of the ozone radiative feedback. *Journal of Geophysical Research: Atmospheres*, 109. https://doi.org/10.1029/2004JD005093

Khaykin, S.M., Funatsu, B.M., Hauchecorne, A., Godin-Beekmann, S., Claud, C., Keckhut, P., Pazmino, A., Gleisner, H., Nielsen, J.K., Syndergaard, S. and Lauritsen, K.B. (2017) Postmillennium changes in stratospheric temperature consistently resolved by GPS radio occultation and AMSU observations. *Geophysical Research Letters*, 44, 7510–7518. https://doi.org/10.1002/2017GL074353

Kim, J., Grise, K. and Son, S.-W. (2013) Thermal characteristics of the cold-point tropopause region in CMIP5 models. *Journal of Geophysical Research*, 118, 8827–8841. https://doi.org/10.1002/jgrd.50649

Laštovička, J., Akmaev, R., Beig, G., Bremer, J. and Emmert, J. (2006) Global change in the upper atmosphere. *Science*, 324, 1253–1254. https://doi.org/10.1126/science.1135134

Lima, L.M., Araújo, L.R., Alves, E.O., Batista, P.P. and Clemesha, B.R. (2015) Variations in meteor heights at 22.7S during solar cycle 23. *Journal of Atmospheric and Solar-Terrestrial Physics*, 133, 139–144. https://doi.org/10.1016/j.jastp.2015.08.015

Lübken, F.-J., Berger, U. and Baumgarten, G. (2009) Stratospheric and solar cycle effects on long-term variability of mesospheric ice clouds. *Journal of Geophysical Research*, 114, D00I06. https://doi.org/10.1029/2009JD012377

Manney, G.L. and Hegglin, M.I. (2018) Seasonal and regional variations of long-term changes in upper-tropospheric jets from reanalyses. *Journal of Climate*, 31, 423–448. https://doi.org/10.1175/JCLI-D-17-0303.1

Manzini, E., Karpechko, A.Y., Anstey, J., Baldwin, M.P., Black, R.X., Cagnazzo, C., Calvo, N., Charlton-Perez, A., Christiansen, B., Davini, P., Gerber, E., Giorgetta, M., Gray, L., Hardiman, S.C., Lee, Y.-Y., Marsh, D.R., McDaniel, B.A., Purich, A., Scaife, A.A.,

Shindell, D., Son, S.-W., Watanabe, S. and Zappa, G. (2014) Northern winter climate change: assessment of uncertainty in CMIP5 projections related to stratosphere–troposphere coupling. *Journal of Geophysical Research: Atmospheres*, 119, 7979–7998. https://doi.org/10.1002/2013JD021403

Marsh, D.R., Mills, M.J., Kinnison, D.E., Lamarque, J.-F., Calvo, N. and Polvani, L.M. (2013) Climate change from 1850 to 2005 simulated in CESM1 (WACCM). *Journal of climate*, 26, 7372–7391. https://doi.org/10.1175/JCLI-D-12-00558.1

Maycock, A.C., Randel, W.J., Steiner, A.K., Karpechko, A.Y., Christy, J., Saunders, R., Thompson, D.W.J., Zou, C.-Z., Chrysanthou, A., Luke Abraham, N., Akiyoshi, H., Archibald, A.T., Butchart, N., Chipperfield, M., Dameris, M., Deushi, M., Dhomse, S., Di Genova, G., Jöckel, P., Kinnison, D.E., Kirner, O., Ladstädter, F., Michou, M., Morgenstern, O., O'Connor, F., Oman, L., Pitari, G., Plummer, D.A., Revell, L.E., Rozanov, E., Stenke, A., Visioni, D., Yamashita, Y. and Zeng, G. (2018) Revisiting the mystery of recent stratospheric temperature trends. *Geophysical Research Letters*, 45, 9919–9933. https://doi.org/10.1029/2018GL078035

Meinshausen, M., Smith, S., Calvin, K.J., Daniel, S., Kainuma, M.L.T., Lamarque, J.-F., Matsumoto, K., Montzka, S.A., Raper, S.C.B., Riahi, K., Thomson, A., Velders, G.J.M. and van Vuuren, D. (2011) The RCP greenhouse gas concentrations and their extensions from 1765 to 2300. *Climatic Change*, 109. https://doi.org/10.1007/s10584-011-0156-z

Molod, A., Takacs, L., Suarez, M., Bacmeister, J., Song, I.-S. and Eichmann, A. (2012). The GEOS-5 Atmospheric General Circulation Model: Mean Climate and Development from MERRA to Fortuna. NASA Technical Report Series on Global Modeling and Data Assimilation, Vol. 28. NASA TM-2012-104606, NASA, Goddard Space Flight Center, Greenbelt, MD. https://gmao.gsfc.nasa.gov/pubs/docs/Molod484.pdf

Molod, A., Takacs, L., Suarez, M. and Bacmeister, J. (2015) Development of the GEOS-5 atmospheric general circulation model: evolution from MERRA to MERRA2. *Geoscientific Model Development*, 8, 1339–1356.

Morgenstern, O., Braesicke, P., O'Connor, F., Bushell, A., Johnson, C., Osprey, S. and Pyle, J. (2009) Evaluation of the new UKCA climate-composition model. Part 1: the stratosphere. *Geoscientific Model Development*, 2, 43–57. https://doi.org/10.5194/gmd-2-43-2009

Morgenstern, O., Zeng, G., Luke Abraham, N., Telford, P.J., Braesicke, P., Pyle, J.A., Hardiman, S.C., O'Connor, F.M. and Johnson, C.E. (2013) Impacts of climate change, ozone recovery, and increasing methane on surface ozone and the tropospheric oxidizing capacity. *Journal of Geophysical Research: Atmospheres*, 118, 1028–1041. https://doi.org/10.1029/2012JD018382

Morgenstern, O., Hegglin, M.I., Rozanov, E., O'Connor, F.M., Abraham, N.L., Akkyoshi, H., Archibald, A.T., Bekki, S., Butchart, N., Chipperfield, M.P., Deushi, M., Dhomse, S.S., Garcia, R.R., Hardiman, S.C., Horowitz, L.W., Jöckel, P., Josse, B., Kinnison, D., Lin, M.Y., Mancini, E., Manyin, M.E., Marchand, M., Marecal, V., Michou, M., Oman, L.D., Pitari, G., Plummer, D.A., Revell, L.E., Saint-Martin, D., Schofield, R., Stenke, A., Stone, K., Sudo, K., Tanaka, T.Y., Tilmes, S., Yamashita, Y., Yoshida, K. and Zeng, G. (2017) Review of the global models used within the Chemistry-Climate Model Initiative (CCMI). *Geoscientific Model Development*, 10, 639–671. https://doi.org/10.5194/gmd-10-639-2017

Morgenstern, O., Stone, K.A., Schofield, R., Akiyoshi, H., Yamashita, Y., Kinnison, D.E., Garcia, R.R., Sudo, K., Plummer, D.A., Scinocca, J., Oman, L.D., Manyin, M.E., Zeng, G., Rozanov, E., Stenke, A., Revell, L.E., Pitari, G., Mancini, E., Di Genova, G., Visioni, D., Dhomse, S.S. and Chipperfield, M.P. (2018) Ozone sensitivity to varying greenhouse gases and ozone-depleting substances in CCMI-1 simulations. *Atmospheric Chemistry and Physics*, 18, 1091–1114. https://doi.org/10.5194/acp-18-1091-2018

Oberländer-Hayn, S., Gerber, E.P., Abalichin, J., Akiyoshi, H., Kerschbaumer, A., Kubin, A., Kunze, M., Langematz, U., Meul, S., Michou, M., Morgenstern, O. and Oman, L.D. (2016) Is the Brewer–Dobson circulation increasing or moving upward?. *Geophysical Research Letters*, 43, 1772–1779. https://doi.org/10.1002/2015GL067545

Oman, L.D., Ziemke, J.R., Douglass, A.R., Waugh, D.W., Lang, C., Rodriguez, J.M. and Nielsen, J.E. (2011) The response of tropical tropospheric ozone to ENSO. *Geophysical Research Letters*, 38. https://doi.org/10.1029/2011GL047865

Oman, L.D., Douglass, A.R., Ziemke, J.R., Rodriguez, J.M., Waugh, D.W. and Nielsen, J.E. (2013) The ozone response to ENSO in Aura satellite measurements and a chemistry–climate simulation. *Journal of Geophysical Research: Atmospheres*, 118, 965–976. https://doi.org/10.1029/2012JD018546

Palmeiro, F.M., Calvo, N. and Garcia, R.R. (2014) Future changes in the Brewer–Dobson circulation under different greenhouse gas concentrations in WACCM4. *Journal of the Atmospheric Sciences*, 71, 2962–2975. https://doi.org/10.1175/JAS-D-13-0289.1

Pitari, G., Aquila, V., Kravitz, B., Robock, A., Watanabe, S., Cionni, I., Luca, N.D., Genova, G.D., Mancini, E. and Tilmes, S. (2014) Stratospheric ozone response to sulfate geoengineering: results from the Geoengineering Model Intercomparison Project (GeoMIP). *Journal of Geophysical Research: Atmospheres*, 119, 2629–2653. https://doi.org/10.1002/2013JD020566

Polvani, L.M., Abalos, M., Garcia, R., Kinnison, D. and Randel, W.J. (2018) Significant weakening of Brewer–Dobson circulation trends over the 21st century as a consequence of the Montreal protocol. *Geophysical Research Letters*, 45, 401–409. https://doi.org/10.1002/2017GL075345

Randel, W.J., Shine, K.P., Austin, J., Barnett, J., Nathan, C.C., Gillett, N.P., Keckhut, P., Langematz, U., Lin, R., Long, C., Mears, C., Miller, A., Nash, J., Seidel, D.J., Thompson, D.W.J., Wu, F. and Yoden, S. (2009) An update of observed stratospheric temperature trends. *Journal of Geophysical Research*, 114, D02 107. https://doi.org/10.1029/2008JD010421

Revell, E.L., Tummon, F., Stenke, A., Sukhodolov, T., Coulon, A., Rozanov, E., Garny, H., Volker, G. and Peter, T. (2015) Drivers of the tropospheric ozone budget throughout the 21st century under the medium-high climate scenario RCP 6.0. *Atmospheric Chemistry and Physics*, 15, 5887–5902. https://doi.org/10.5194/acp-15-5887-2015

Sausen, R. and Santer, B.D. (2003) Use of changes in tropopause height to detect human influences on climate. *Meteorologische Zeitschrift*, 12, 131–136. https://doi.org/10.1127/0941-2948/2003/0012-0131

Schmidt, H., Brasseur, G.P., Charron, M., Manzini, E., Giorgetta, M.A., Diehl, T., Fomichev, V.I., Kinnison, D., Marsh, D. and Walters, S. (2006) The HAMMONIA chemistry climate model: sensitivity of the mesopause region to the 11-year solar cycle and

CO_2 doubling. *Journal of Climate*, 19, 3903–3931. https://doi.org/10.1175/JCLI3829.1

Scinocca, J., McFarlane, N., Lazare, M., Li, J. and Plummer, D. (2008) Technical note: the CCCma third-generation AGCM and its extension into the middle atmosphere. *Atmospheric Chemistry and Physics*, 8, 7055–7074. https://doi.org/10.5194/acp-8-7055-2008

Seidel, D.J. and Randel, W.J. (2006) Variability and trends in the global tropopause estimated from radiosonde data. *Journal of Geophysical Research*, 111(D21 101). https://doi.org/10.1029/2006JD007363

Shepherd, T.G. and McLandress, C. (2011) A robust mechanism for strengthening of the Brewer–Dobson circulation in response to climate change: critical-layer control of subtropical wave breaking. *Journal of Atmospheric Sciences*, 68, 784–797. https://doi.org/10.1175/2010JAS3608.1

Singh, M.S. and O'Gorman, P.A. (2012) Upward shift of the atmospheric general circulation under global warming. *Journal of Climate*, 25, 8259–8276. https://doi.org/10.1175/JCLI-D-11-00699.1

Solomon, S., Kinnison, D., Bandoro, J. and Garcia, R. (2015) Simulation of polar ozone depletion: an update. *Journal of Geophysical Research: Atmospheres*, 120, 7958–7974. https://doi.org/10.1002/2015JD023365

SPARC (2010) *SPARC CCMVal Report on the Evaluation of Chemistry-Climate Models*. In: Eyring, V., Shepherd, T.G., and Waugh, D.W. (Eds.) WCRP-132, WMO/TD-1526, SPARC Report No. 5. SPARC Office. https://www.sparc-climate.org/publications/sparc-reports/sparc-report-no-5/; accessed 28 July 2020.

Stenke, A., Schraner, M., Rozanov, E., Egorova, T., Luo, B. and Peter, T. (2013) The SOCOL version 3.0 chemistry–climate model: description, evaluation, and implications from an advanced transport algorithm. *Geoscientific Model Development*, 6, 1407–1427. https://doi.org/10.5194/gmd-6-1407-2013

Stober, G., Matthias, V., Brown, P. and Chau, J.L. (2014) Neutral density variation from specular meteor echo observations spanning one solar cycle. *Geophysical Research Letters*, 41, 6919–6925. https://doi.org/10.1002/2014GL061273

Stone, K., Morgenstern, O., Karoly, D., Klekociuk, A., French, W., Abraham, N. and Schofield, R. (2016) Evaluation of the Australian community climate and earth-system simulator chemistry–climate model. *Atmospheric Chemistry and Physics*, 16, 2401–2415. https://doi.org/10.5194/acp-16-2401-2016

Taylor, K.E., Stouffer, R.J. and Meehl, G.A. (2012) An overview of CMIP5 and the experiment design. *Bulletin of the American Meteorological Society*, 93, 485–498. https://doi.org/10.1175/BAMS-D-11-00094.1

Vallis, G.K., Zurita, P., Cairns, C. and Kidston, J. (2015) Response of the large-scale structure of the atmosphere to global warming. *Quarterly Journal of the Royal Meteorological Society*, 141, 1479–1501. https://doi.org/10.1002/qj.2456

Šácha, P., Eichinger, R., Garny, H., Pišoft, P., Dietmüller, S., de la Torre, L., Plummer, D.A., Jöckel, P., Morgenstern, O., Zeng, G., Butchart, N. and Añel, J.A. (2019) Extratropical age of air trends and causative factors in climate projection simulations. *Atmospheric Chemistry and Physics*, 19, 7627–7647. https://doi.org/10.5194/acp-2018-1310

WMO (2011) Global Ozone Research and Monitoring Project-Report No. 52. Scientific Assessment of Ozone Depletion: 2010; https://www.esrl.noaa.gov/csl/assessments/ozone/2010/citations.html; accessed 28 July 2020.

Yukimoto, S., Yoshimura, H., Hosaka, M., Sakami, T., Tsujino, H., Hirabara, M., Tanaka, T., Deushi, M., Obata, A., Nakano, H., Adachi, Y., Shindo, E., Yabu, S., Ose, T. and Kitoh, A. (2011) *Meteorological Research Institute-Earth System Model Version 1 (MRI-ESM1) – Model Description –*. Technical Reports of the Meteorological Research Institute No. 64. JMA, Tokyo, Japan: Meteorological Research Institute. https://www.mri-jma.go.jp/Publish/Technical/DATA/VOL_64/tec_rep_mri_64.pdf

Yukimoto, S., Adachi, Y., Hosaka, M., Sakami, T., Yoshimura, H., Hirabara, M., Tanaka, T.Y., Shindo, E., Tsujino, H., Deushi, M., Mizuta, R., Yabu, S., Obata, A., Nakano, H., Koshiro, T., Ose, T. and Kitoh, A. (2012) A new global climate model of the Meteorological Research Institute: MRI-CGCM3 model description and basic performance. *Journal of the Meteorological Society of Japan. Ser. II*, 90, 23–64.

SUPPORTING INFORMATION

Additional supporting information may be found online in the Supporting Information section at the end of this article.

How to cite this article: Eichinger R, Šácha P. Overestimated acceleration of the advective Brewer–Dobson circulation due to stratospheric cooling. *QJR Meteorol Soc*. 2020;1–15. https://doi.org/10.1002/qj.3876